Optical trapping of large metallic particles in air

S. Mirzaei-Ghormish, S. Griffith, D. Smalley,* and Ryan M. Camacho
Department of Electrical and Computer Engineering, Brigham Young University, Provo, Utah 84602, USA

(Received 1 September 2023; revised 16 May 2024; accepted 5 November 2024; published 11 December 2024)

In this paper, we introduce a horizontally oriented photophoretic "boat" trap that is capable of capturing and self-loading the largest reported (radius $\geq$1 μm) photophoreticaly trapped solid gold particles in air for more than 1 h. Once trapped, particles are held stably, without hopping, even as the trap is modified to scan axially or expanded to a larger size to increase the capture cross section. We theoretically present and experimentally demonstrate each of these affordances.

DOI: 10.1103/PhysRevApplied.22.064042

I. INTRODUCTION

Plasmonic particles exhibit unique properties, such as strong and broad light-matter interactions, fluorescence, and photocatalysis [1]. These attributes render them highly effective in enhancing levitated optomechanical systems. Owing to their strong interaction with light and high densities, large solid-metallic particles offer solutions to mitigate hopping issues and enhance the quality of optical-trap displays [2]. These particles could also increase the sensitivity of detection of airborne pathogens, improve experiments on the catalysis of gaseous chemical reactions [3], and bring plasmonic field enhancement to a host of levitated optical systems. Moreover, systems involving trapped plasmonic particles can facilitate the observation of new physics by offering enhanced isolation from the environment and extending their operation into three-dimensional (3D) space [4]. However, it has proven notoriously difficult to robustly trap large metallic particles in air. For large metallic particles exposed to laser light, optical forces are mainly driven by positive photophoretic forces. Unlike smaller metallic nanoparticles, the plasmonic absorption spectrum shifts to longer wavelengths and broadens [5,6], causing uneven heating on the illuminated particle side. Due to the Soret effect, this creates a positive photophoretic force that pushes the particle from hotter to colder regions, overpowering other forces. Consequently, these particles are trapped at intensity minima, unlike smaller or less-absorbent particles that can be trapped at intensity maxima due to negative photophoretic or gradient forces [7].

All known efforts to optically trap metallic particles away from surfaces are shown in Fig. 1(a) [5,8–20]. We calculate the photophoretic force and extinction cross section for each particle based on its reported size and material. The extinction cross section encompasses both scattering and absorption, contributing to repulsion. The data point size reflects the particle size, while red markers indicate air-trapped particles and blue markers indicate water-trapped ones. The calculations assume spherical shapes, though nonspherical shapes are expected to reduce repulsive forces [5].

Several key observations can be made. First, larger metallic particles experience greater repulsive radiation and photophoretic forces, as anticipated. Second, photophoretic forces decrease when particles are in water. Notably, all trapped metallic particles to date have operated in regimes in which attractive forces prevail or thermal effects are negated, highlighting the need for new air-trapping geometries for large metallic particles.

Further details reveal that metallic particles have been trapped in both water and air using inverted optical tweezers in the dipole regime [radius (R) $\ll$ wavelength] [5,8–12]. Here, trapping relies on attractive gradient forces, overshadowing repulsive scattering and thermal forces. However, such methods can dramatically heat the particle surface beyond the melting point, limiting utility. In the Mie regime (radius $\geq$ wavelength), repulsive forces may destabilize the particles. Reflective coatings can mitigate Soret effects [13,14]. Mie particles have also been trapped in two dimensions (2D) or loosely in 3D with engineered beams in water, with size limitations [15–20]. Trapping near extreme fields at surfaces has also been reported [21]. For applications that require free-space axial and radial movement (such as displays), new approaches to air trapping of large metallic particles are needed.

We finally note that several previous experiments have successfully trapped nonmetallic absorbing particles photphoretically using optical beams with local intensity aberrations [22–25], leading to demonstrations of, e.g., 3D volumetric displays [2]. The density of metallic particles is much larger than that of nonmetallic particles (carbon,

*Contact author: smalley@byu.edu

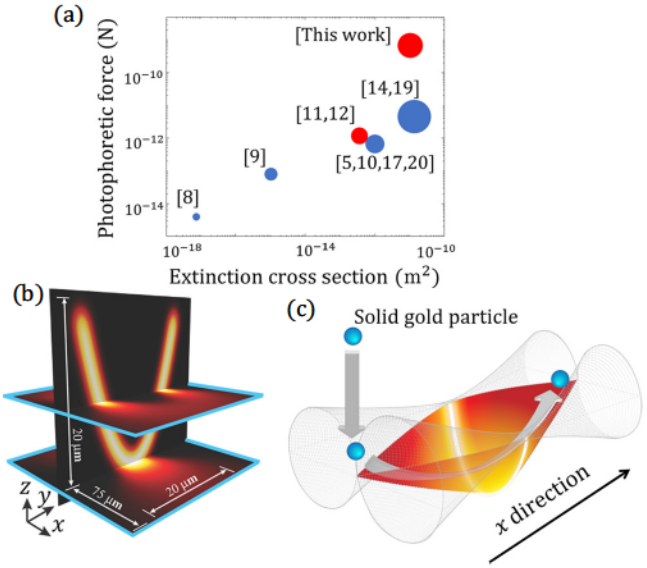

FIG. 1. (a) The illustrated contribution of this work, by comparing the calculated photophoretic force and extinction cross section of published experimental optical trapping of metallic particles in air and water. (b) The 3D boat-shaped intensity distribution of the trap reported in this work. (c) This boat trap shows a self-loading operation for metallic particles.

soot, black liquor), making trapping more difficult. At the same time, photophoretic forces in similarly sized metallic particles are 1–2 orders of magnitude larger, which has the potential to mitigate or further complicate this difficulty. The result of these differences is that, in our experiments, the local trap sites created by speckle and aberration that are capable of routinely trapping nonmetallic particles (such as soot) have not been able to hold the metallic particles. An alternative trapping method is required.

This work demonstrates for the first time the trapping of large gold particles in air without proximity to a surface. Solid gold particles have demonstrated trap lifetimes in excess of 1 h. Our trap design builds on previous work demonstrating arbitrary acousto-optic control of optical-trapping beams [26,27] and a resulting 3D morphology that allows for near-solid-state axial and lateral translation [28]. Our design also has an unexpected and convenient photophoretic (rather than gravitational) self-loading phenomenon not previously reported and the ability to dynamically change the trapping potential and location [Fig. 1(a)]. This enables, simultaneously, a large capture cross section and a singular stable-trap locus with an overall action reminiscent of loading within a mechanical pencil. The dynamic nature of the trap also allows for adjustment of the absolute location of the self-loading terminus—providing a possible solution to the challenge of variability in other self-loading systems [29]. These particles used in this experiment have been obtained commercially. Their mean diameter is 1.16 μm (standard deviation 0.512 μm and diameter sphericity of 0.94). To explain the underlying physics of our trap, we present a theoretical model of the dynamical trap in terms of all relevant optical forces. Using our model, we calculate the trapping potential in the transverse and propagation planes and show the self-loading operation. Our theory is in good agreement with experimental observations.

II. TRAP DESIGN

To achieve a 3D photophoretic trap for metallic particles, we form a dynamic repulsive energy well by rapidly scanning a focused laser along a parabolic path in the y-z plane (transverse plane), as depicted in Fig. 1(b). If the scan rate exceeds the diffusional motion of the particle, the particle senses a quasistatic repulsive intensity distribution. Details on achieving uniform side walls can be found in the Supplemental Material [30].

It is straightforward to see that the scanning laser forms a parabolic well in the transverse plane. What is less obvious but crucial is how it also creates a deep trapping potential along the x axis (propagation direction). As illustrated in Fig. 1(b), the quasistatic electric field has two nearly parallel diverging Gaussian beams, the intensity of which resembles a boat shape. The intensity peaks along the x axis are due to the overlap of these beams at two points: the stern and the bow of the "boat." We call these convergence points, and they repel particles to the center of the boat. Although the electric field is x-axis symmetric, the photophoretic force is not, as the laser illuminates the particle from one side. Interestingly, due to beam divergence, the opposite side of the particle can be preferentially illuminated at the positive convergence point. This enables a single laser to push a particle in the $-x$ direction, despite propagating in the $+x$ direction. This also implies that the potential minimum of the trap will be near this positive convergence point. The superposition of all beams results in a 3D boat-shaped potential, shown in Fig. 1(c).

The intensity in the transverse plane at time t may be expressed as $z_f(t) = (2/d)\, y_f^2(t) - d$, where $-d \le y_f(t) \le d$ is the tuning parameter that controls the size of the potential trap in both the transverse and axial planes. The dynamic intensity is

$$I(x,y,z;t) = \left(\frac{2p_{\text{in}}}{\pi w^2(x)}\right) e^{-2\left(\frac{(z-z_f(t))^2+(y-y_f(t))^2}{w^2(x)}\right)}, \quad (1)$$

where $w(x) = w_0\sqrt{1+(x/x_0)^2}$ is the beam width, $w_0 = \frac{2\lambda}{\pi \text{NA}}$ is the beam waist, NA is the numerical aperture, $x_0 = k_0 w_0^2/2$ is the Rayleigh length, and p_{in} is the laser power; the focal point of the laser beam is located at the $x = 0$ plane. To create a uniform intensity, the speed of the

scanner is adjusted to be constant along the parabolic path, as described in the Supplemental Material [30].

Particles are trapped inside the dark region of the boat by repulsion from the surrounding intensity barrier. The trap is adiabatic and its volume can be adjusted using the parameter d, controlled by the radio frequency of the acousto-optic modulators (AOMs). The dimensions of the boat—width $W = 2d$, depth $H = 2d$, and length $L = (k_0\omega_0)\sqrt{y_1^2 - w_0^2}$ [where $y1 = \sqrt{d/2(w_0 + R)}$]—are specified in Fig. S1 of the Supplemental Material [30]. Both the width and the height depend solely on d, while the length also depends on the NA. Increasing d expands the volume of the boat and a higher NA compresses it axially. A larger boat holds more particles, while a smaller one offers a deeper potential.

III. THEORETICAL CALCULATION OF TRAPPING FORCES

We model the boat trap by calculating all relevant optical and thermal forces and their corresponding energy potentials. The effect of Langevin forces, including Brownian motion, is considered by comparing the depth of the potential traps with thermal energy k_BT. Here, we neglect the drag force, as it is small compared to the optical and thermal forces. The details of the calculations are shown in the Supplemental Material [30].

In the transverse plane, we calculate the total forces (optical and photophoretic forces) and the potential trap on the line $z = (2/d)\,y^2 - d + (\omega_0 + R)$. This path follows the $1/e^2$ intensity point of the Gaussian beams relative to the y-z plane, offset by the radius of the particle, In Figs. 2(a) and 2(b), the total force in the y and z directions and the transverse potential trap are shown as a function of angle θ at $x = 0$. Since the y component of the total force is an odd function of θ, where it is negative for $0 \le \theta \le \pi/2$ and positive for $-\pi/2 \le \theta \le 0$, the particle is continuously pulled into the trap region in the y direction. In contrast, the z component of the total force is an even function of θ and its values are positive. This means that the particle experiences repulsive forces in the z direction that overcome gravity. The vector map of the total force in the transverse plane is shown in the Supplemental Material [30]. The potential energy of the trap at point $\rho = (y, z)$ is

$$U(\rho) = -\int_{\infty}^{\rho} \vec{F}_{tot} \cdot d\vec{\rho} = -\int_{\infty}^{y} \left(F_y + \frac{4}{d} F_z y'\right) dy'. \quad (2)$$

The potential $U(\rho)$ is depicted in Fig. 2(b), showing a symmetric trap in the transverse plane with a minimum at $\theta = 0$ ($y = 0$). To counteract Brownian motion, the trap depth $U_{\min}$ is $5500k_BT$ (10 times the thermal energy), ensuring stability. Similar calculations for successive x values yield a 3D potential $U(x, y, z)$.

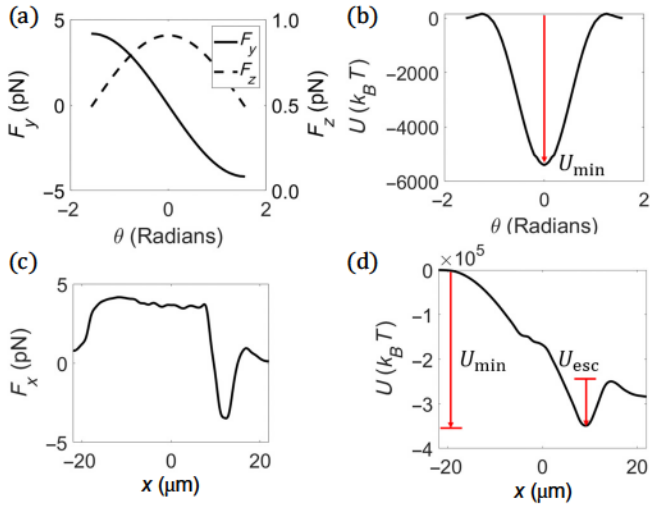

FIG. 2. (a) The y and z components of the total force and (b) the potential trap in the transverse plane. (c) The total force and (d) the potential trap in the longitudinal direction. The simulation parameters are chosen as follows: $\lambda = 532$ nm, $p_{in} = 10$ mW, NA $= 0.15$, $\omega = 5$ kHz, $R = 1$ μm, and $d = 5$ μm. The optical forces are found by numerically calculating the Maxwell stress tensor using Eq. S4 in the Supplemental Material [30] (from Ref. [31]) and the photophoretic force is calculated using Eq. S7 in the Supplemental Material [30] (from Ref. [32]).

In the axial direction, we evaluate the potential along a path at $z = w(x) + R$, aligned with the $1/e^2$ intensity of the Gaussian beams and offset by the particle radius. To reduce the computational load, we focus on nearby electric field regions. The beam size vastly exceeds the particle size ($w_0 >> R$), allowing us to approximate the field as the sum of three discrete beams, detailed in Fig. S1 of the Supplemental Material [30]. Their focal points are at $(0, y1, -d + w_0 + R)$, $(0, 0, -d)$, and $(0, -y1, -d + w_0 + R)$, converging at $x = \pm 13$ μm.

Then, the potential energy of the trap at point (x, z) is

$$U(x) = -\int_{\infty}^{x} \left(F_x + \frac{\omega_0^2}{x_0^2} \frac{x'}{\omega(x')} F_z\right) dx'. \quad (3)$$

In Figs. 2(c) and 2(d), we illustrate the axial force and the potential trap. For $x < 0$, the force is positive, indicating repulsion toward the focus. For $x > 0$, the force initially remains positive but turns negative near the positive convergence point. This negative force in the $9\ \mu\text{m} \le x \le 15\ \mu\text{m}$ region leads to particle trapping. The resulting potential is asymmetric, centered near $x = 9$ μm, and has sufficient depth ($U_{\min} = 350\,000k_BT$) and potential barrier ($U_{esc} = 1000k_BT$) to counter Brownian motion, ensuring stable trapping. Combined with the transverse potentials shown in Figs. 2(b) and 2(d), the equilibrium lies near the positive convergence point near the "center bow" of the boat.

IV. EXPERIMENTAL DEMONSTRATION

Experiments have been performed to validate the theoretical predictions of the previous section and demonstrate the advantages of the proposed boat-shaped trap. A top view of the experimental setup is shown in Fig. 3. A linearly polarized Gaussian beam derived from a cw coherent laser source (Verdi-V10, $\lambda = 532$ nm) passes through a pair of AOMs. The AOMs are driven by a Rigol DG4202 arbitrary waveform generator with a voltage-controlled oscillator (VCO) and amplifiers. The incoming light passing through AOM1 is diffracted, where the zero-order (solid line) and first-order (dashed line) diffracted beams have the highest diffraction efficiency. The zero-order beam is an undeflected point beam and the first-order beam scans space in the z direction [inset (a)]. These beams then pass through AOM2, where they are again diffracted into beams 1, 2, 3, and 4 [inset (b)]. Beams 1 and 4, respectively, scan space in the y and z directions. Beam 3 is a point and beam 2 scans space with a parabolic path. An iris is then used to pass only beam 2, the transverse and axial profiles of which are shown in inset (c). Two sets of relay lenses, (L_1, L_2) and (L_3, L_4), optically superimpose and collimate the beams so that they share a common origin of angular deflection. A white-light source (WLS) provides background illumination for the images of the particles at the CCD2 camera. The 50% beam splitter (BS) combines laser light with white light. The notch filter (NF) cuts the laser radiation, and the microscope objective (MO) focuses the boat trap on the trap site. The CCD1 camera visualizes the dynamics of the trapped particle in the axial plane (side view) and CCD2 visualizes it in the transverse plane (front view). To create the nonuniform intensity distribution, the radio frequency of AOM1 is twice the radio frequency of AOM2, and for the uniform distribution, the radio frequencies of both AOMs are equal, with a relative phase shift. The instantaneous power of the scanning beam is 1 W but the particle experiences a 10-mW averaged power at each point over the parabolic path. The trapping region is enclosed by a 2×1 cm^2 glass tube to reduce the airflow around the trap site. Particle loading is performed by releasing particles from the top of the glass tube into the trapping region, where they are observed using CCD1 and CCD2. For example, the trapped gold particles are visualized by CCD1 and CCD2 in insets (d) and (e), respectively. (We note that, from the perspective of CCD2, the solid gold particles had poor visibility when trapped. Therefore, for illustration purposes, a large gold-coated microsphere has been used in this image.)

Our trap system provides full control over the dynamics of the trapped particle, including self-loading, modulation, and translation. In Fig, 4(a) and Video 1, we show the self-loading operation of particles into the trapping region, resulting in a trapped particle near the positive convergence point as predicted by our theoretical analysis. The laser is scanned at a rate of 2 kHz in the uniform distribution setting and the tuning parameter is chosen to be $d = 50$ μm. The trapping region, where the potential energy well can capture particles, is indicated by the yellow oval. The position of a single particle that is eventually trapped is indicated at different time steps $x(t)$ with red arrows. When the particle enters the trapping region, it is guided to a single stable-trap point as shown by the three frames t_1, t_2, and t_3. This trapping behavior agrees with our theoretical calculations, which predict that in the transverse plane, the particles are confined near the axis of symmetry and in the axial plane they are pushed from the left side of the boat trap toward the right side of the boat trap before becoming trapped to the right of the focal plane.

The numerical computation of the photophoretic force is computationally intensive due to the interplay of electromagnetic absorption and heat-transfer equations (see the Supplemental Material [30]). For instance, calculating the temperature distribution for a single particle location has

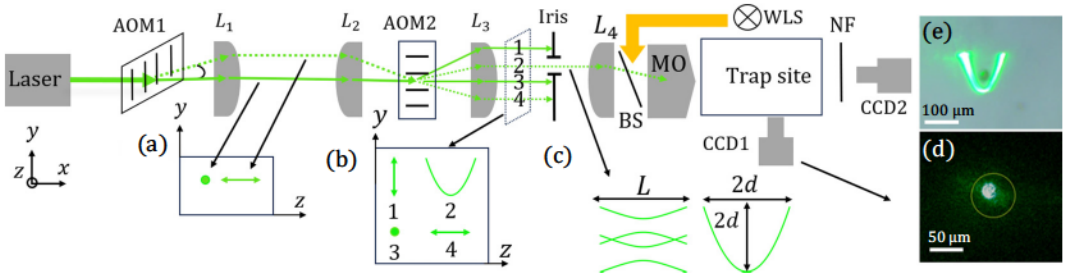

FIG. 3. The schematic diagram of the experimental setup from a top view. The dynamic boat-shaped intensity is created by a pair of AOMs, where the first AOM scans light in the z direction [inset (a)] and the second AOM in the y direction [inset (b)], resulting in a boat-shaped trap [inset (c)]. Two sets of relay lenses, (L_1, L_2) and (L_3, L_4), optically superimpose and collimate the beams so that they share a common origin of angular deflection. The CCD1 [inset (e)] and CCD2 [inset (d)] cameras visualize the dynamics of the trapped particle in side and front views. The yellow circle in inset (d) is an annotation added at the time of image capture, showing where we have estimated the focal point of the beam. The iris is used to pass the boat-shaped beam and the notch filter (NF) protects the camera.

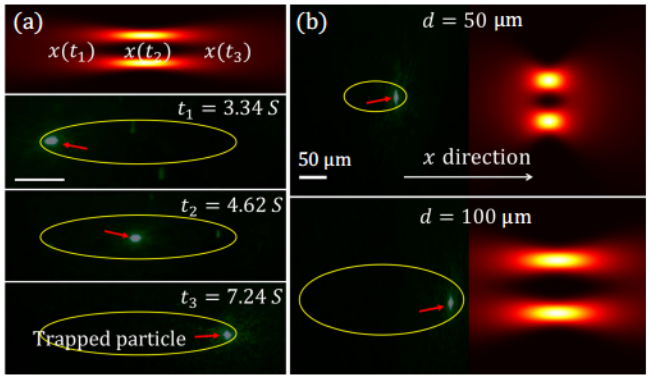

FIG. 4. (a) The self-loading operation for uniform intensity distribution at 2 kHz and $d = 50$ µm. (b) The modulation operation by changing d from 50 µm to 100 µm.

required a mesh with 204 747 points and has taken 9 h on an eight-core Intel i7-10875H CPU. To mitigate this, we have numerically focused on a trap with $d = 5\,\mu m$. Our calculations accurately predict stable points for varying d. For $d = 50\,\mu m$, the positive convergence point is at $x = 106\,\mu m$, aligning well with experimental measurements of $x = 102\,\mu m$. The images are cropped and contrast enhanced for clarity.

Various trapping parameters can be adiabatically adjusted for real-time 3D control of the particle position and velocity. The trap volume depends on the tuning-voltage range of the VCO and parameter d, which also affects the trapping-region dimensions H and L. In Fig. 4(b) and Video 1, the trap volume increases as d changes from 50 µm to 100 µm, altering the z and x coordinates of the trapping point. Experimental observations confirm that increasing d extends the distance from the trap to the focal point. In addition, the translation operation is discussed in the Supplemental Material [30]. In the translation operation, the trap volume remains constant but it moves longitudinally to a desired location. In this scenario, the height of the trap point remains unchanged and only the position of the trap point is adjusted along the longitudinal direction.

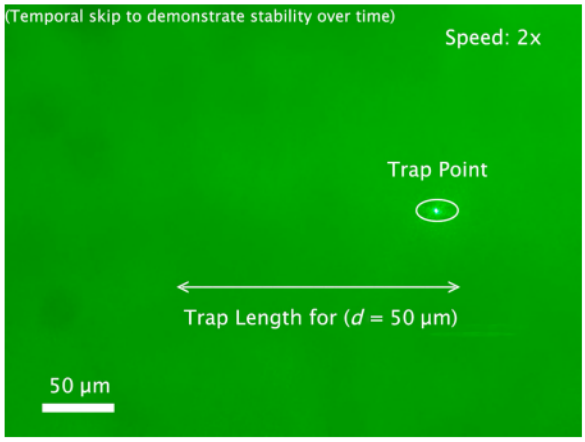

VIDEO 1. Particle self-loading and translation.

The trap lifetimes as a function of the scan rate for 1-µm solid gold particles are shown in the Supplemental Material [30]. As shown in Fig. S3(b) of the Supplemental Material [30], the trap lifetimes exceed 1 h at the scan rate of 20 kHz. The trap lifetime is correlated with the scan rate. To better understand the effect of the scanning rate on the trapping, we have conducted an experiment using 30-µm gold and carbon-coated microparticles (see Fig. S4 in the Supplemental Material [30]). For each scan rate, we have recorded the repeated experiment several hundred times, with lifetimes capped above 100 s. The dashed red lines indicate the average lifetimes. The normalized trap lifetime increases as the scan rate increases from 0.1 kHz to 20 kHz. However, due to chirping, it gradually decreases as the scan rate increases to 100 kHz (for more details, see the Supplemental Material [30]).

V. DISCUSSION

A discussion of the utility of the resulting boat trap follows.

This work presents a boat-trap design for enhanced particle control in optical-trapping systems. The boat trap offers self-loading capabilities, precise modulation, and translation, addressing shortcomings of existing photophoretic traps that often exhibit arbitrary particle distribution and spontaneous hopping [22–25]. The deep potential well of this trap ensures stable particle positioning with minimal oscillations.

The self-loading mechanism of the boat trap overcomes the typical challenges of loading particles into optical traps in air. Unlike liquid environments, air-based traps lack buoyancy and present gravitational complications. Obviating the need for interventions such as differential pumping, precooling, and feedback systems to enhance trapping efficiency [33], this trap provides a larger capturing domain and photophoretic particle guidance, simplifying the loading process. Additionally, dynamic trap adjustment allows fine tuning of the self-loading terminus, making it adaptable to potential loading variability.

Photophoresis enables single-axis particle manipulation, resembling the concept of a tractor beam. This distinguishes it from Paul, Penning, electrophoretic, and acoustophoretic traps, which require multiaxis fields. This single-axis requirement enables long-distance manipulation without external interference, making the trap ideal for hop-free free-space volumetric displays and for precision pointing and placement applications such as the aerial colocation of levitated nitrogen-vacancy- (N-V) center nanodiamonds and gold particles to study plasmonic field enhancement or nanoscale thermal radiation [34].

VI. CONCLUSIONS

This work demonstrates the successful optical trapping of large metallic particles using a method based on positive photophoretic forces. The boat trap ensures a predictable trap location and high trapping probability. Its dynamic nature enables axial scanning and an increased particle trap count. These advancements offer enhanced particle illumination and control, paving the way for improved image quality in optical-trap displays and new investigations into light-matter interactions.

ACKNOWLEDGMENTS

We acknowledge financial support from the National Science Foundation (Grant No. 2234534). We also thank Spencer Duke for his contributions to the paper.

[1] H. Yu, Y. Peng, Y. Yang, and Z.-Y. Li, Plasmon-enhanced light-matter interactions and applications, npj Comput. Mater. **5**, 45 (2019).

[2] D. Smalley, E. Nygaard, K. Squire, J. Van Wagoner, J. Rasmussen, S. Gneiting, K. Qaderi, J. Goodsell, W. Rogers, M. Lindsey *et al.*, A photophoretic-trap volumetric display, Nature **553**, 486 (2018).

[3] Y. Zheng, Q. Zhuang, Y. Ruan, and B. Wei, Acoustic levitation synthesis and subsequent physicochemical properties of bimetallic composite nanoparticles, Appl. Phys. Lett. **122**, 084102 (2023).

[4] C. Gonzalez-Ballestero, M. Aspelmeyer, L. Novotny, R. Quidant, and O. Romero-Isart, Levitodynamics: Levitation and control of microscopic objects in vacuum, Science **374**, eabg3027 (2021).

[5] O. Brzobohatỳ, M. Šiler, J. Trojek, L. Chvátal, V. Karásek, A. Paták, Z. Pokorná, F. Mika, and P. Zemánek, Three-dimensional optical trapping of a plasmonic nanoparticle using low numerical aperture optical tweezers, Sci. Rep. **5**, 8106 (2015).

[6] N. G. Khlebtsov and L. A. Dykman, Optical properties and biomedical applications of plasmonic nanoparticles, J. Quant. Spectrosc. Radiat. Transfer **111**, 1 (2010).

[7] O. Jovanovic, Photophoresis—Light induced motion of particles suspended in gas, J. Quant. Spectrosc. Radiat. Transfer **110**, 889 (2009).

[8] K. Svoboda and S. M. Block, Optical trapping of metallic Rayleigh particles, Opt. Lett. **19**, 930 (1994).

[9] Y. Seol, A. E. Carpenter, and T. T. Perkins, Gold nanoparticles: Enhanced optical trapping and sensitivity coupled with significant heating, Opt. Lett. **31**, 2429 (2006).

[10] P. M. Hansen, V. K. Bhatia, N. Harrit, and L. Oddershede, Expanding the optical trapping range of gold nanoparticles, Nano Lett. **5**, 1937 (2005).

[11] L. Jauffred, S. M.-R. Taheri, R. Schmitt, H. Linke, and L. B. Oddershede, Optical trapping of gold nanoparticles in air, Nano Lett. **15**, 4713 (2015).

[12] Y. Arita, G. Tkachenko, N. McReynolds, N. Marro, W. Edwards, E. R. Kay, and K. Dholakia, Invited Article: Optical trapping of ultrasmooth gold nanoparticles in liquid and air, APL Photonics **3**, 070801 (2018).

[13] A. Ashkin and J. Dziedzic, Stability of optical levitation by radiation pressure, Appl. Phys. Lett. **24**, 586 (1974).

[14] G. Roosen and C. Imbert, The TEM*01 mode laser beam—A powerful tool for optical levitation of various types of spheres, Opt. Commun. **26**, 432 (1978).

[15] K. Sasaki, M. Koshioka, H. Misawa, N. Kitamura, and H. Masuhara, Optical trapping of a metal particle and a water droplet by a scanning laser beam, Appl. Phys. Lett. **60**, 807 (1992).

[16] S. Sato, Y. Harada, and Y. Waseda, Optical trapping of microscopic metal particles, Opt. Lett. **19**, 1807 (1994).

[17] H. Furukawa and I. Yamaguchi, Optical trapping of metallic particles by a fixed Gaussian beam, Opt. Lett. **23**, 216 (1998).

[18] P. C. Ke and M. Gu, Characterization of trapping force on metallic Mie particles, Appl. Opt. **38**, 160 (1999).

[19] A. T O'Neil and M. J. Padgett, Three-dimensional optical confinement of micron-sized metal particles and the decoupling of the spin and orbital angular momentum within an optical spanner, Opt. Commun. **185**, 139 (2000).

[20] M. Gu and D. Morrish, Three-dimensional trapping of Mie metallic particles by the use of obstructed laser beams, J. Appl. Phys. **91**, 1606 (2002).

[21] Y. Zhang, C. Min, X. Dou, X. Wang, H. P. Urbach, M. G. Somekh, and X. Yuan, Plasmonic tweezers: For nanoscale optical trapping and beyond, Light: Sci. Appl. **10**, 59 (2021).

[22] V. G. Shvedov, A. V. Rode, Y. V. Izdebskaya, A. S. Desyatnikov, W. Krolikowski, and Y. S. Kivshar, Selective trapping of multiple particles by volume speckle field, Opt. Express **18**, 3137 (2010).

[23] V. G. Shvedov, C. Hnatovsky, A. V. Rode, and W. Krolikowski, Robust trapping and manipulation of airborne particles with a bottle beam, Opt. Express **19**, 17350 (2011).

[24] Z. Zhang, D. Cannan, J. Liu, P. Zhang, D. N. Christodoulides, and Z. Chen, Observation of trapping and transporting air-borne absorbing particles with a single optical beam, Opt. Express **20**, 16212 (2012).

[25] Z. Gong, Y.-L. Pan, and C. Wang, Optical configurations for photophoretic trap of single particles in air, Rev. Sci. Instrum. **87**, 103104 (2016).

[26] N. Friedman, L. Khaykovich, R. Ozeri, and N. Davidson, Compression of cold atoms to very high densities in a rotating-beam blue-detuned optical trap, Phys. Rev. A **61**, 031403 (2000).

[27] V. Milner, J. Hanssen, W. Campbell, and M. Raizen, Optical billiards for atoms, Phys. Rev. Lett. **86**, 1514 (2001).

[28] Z. Gong, Y.-L. Pan, G. Videen, and C. Wang, Optical trapping and manipulation of single particles in air: Principles, technical details, and applications, J. Quant. Spectrosc. Radiat. Transfer **214**, 94 (2018).

[29] R. A. Kirian, S. Awel, M. Wiedorn, D. Horke, N. Roth, N. O. Eckerskorn, J. Küpper, H. N. Chapman, and A. V. Rode, in *Optical Trapping and Optical Micromanipulation XIII* (SPIE, San Diego, California, United States, 2016), Vol. 9922, p. 84.

[30] See the Supplemental Material at http://link.aps.org/supplemental/10.1103/PhysRevApplied.22.064042 for more information about the intensity distribution of the scanning laser, and the calculation of the optical and thermal forces.

[31] L. Novotny and B. Hecht, *Principles of Nano-Optics* (Cambridge University Press, Cambridge, UK, 2012).

[32] W. Zulehner and H. Rohatschek, Representation and calculation of photophoretic forces and torques, J. Aerosol Sci. **26**, 201 (1995).

[33] J. Gieseler, J. R. Gomez-Solano, A. Magazzù, I. P. Castillo, L. P. García, M. Gironella-Torrent, X. Viader-Godoy, F. Ritort, G. Pesce, A. V. Arzola *et al.*, Optical tweezers—from calibration to applications: A tutorial, Adv. Opt. Photonics **13**, 74 (2021).

[34] P.-O. Chapuis, B. J. Lee, and A. Rodriguez, Thermal radiation at the nanoscale and applications, Appl. Phys. Lett. **123**, 220401 (2023).